Atmos. Chem. Phys. Discuss., 14, 20159–20195, 2014
www.atmos-chem-phys-discuss.net/14/20159/2014/
doi:10.5194/acpd-14-20159-2014

Atmospheric Chemistry and Physics Discussions

Transport pathways of peroxyacetyl nitrate in the upper troposphere and lower stratosphere from different monsoon systems during the summer monsoon season

S. Fadnavis[1], K. Semeniuk[2], M. G. Schultz[3], A. Mahajan[1], L. Pozzoli[4], S. Sonbawane[1], and M. Kiefer[5]

[1]Indian Institute of Tropical Meteorology, Pune, India
[2]Department of Earth and Space Sciences and Engineering, York University, Toronto, Canada
[3]Institute for Energy and Climate Research-Troposphere (IEK-8), Forschungszentrum Jülich, Jülich, Germany
[4]Eurasia Institute of Earth Sciences, Istanbul Technical University, Istanbul, Turkey
[5]Karlsruhe Institute of Technology, Institute for Meteorology and Climate Research, Karlsruhe, Germany

Received: 5 June 2014 – Accepted: 14 July 2014 – Published: 4 August 2014

Correspondence to: S. Fadnavis (suvarna@tropmet.res.in)

Published by Copernicus Publications on behalf of the European Geosciences Union.

Discussion Paper | Discussion Paper | Discussion Paper | Discussion Paper |

Abstract

The Asian summer monsoon involves complex transport patterns with large scale redistribution of trace gases in the upper troposphere and lower stratosphere (UTLS). We employ the global chemistry–climate model ECHAM5-HAMMOZ in order to evaluate the transport pathways and the contributions of nitrogen oxide reservoir species PAN, NO_x, and HNO_3 from various monsoon regions, to the UTLS over Southern Asia and vice versa. The model is evaluated with trace gas retrievals from the Michelson Interferometer for Passive Atmospheric Sounding (MIPAS-E) and aircraft campaigns during the monsoon season (June–September).

There are three regions which contribute substantial pollution to the UTLS during the monsoon: the Asian summer monsoon (ASM), the North American Monsoon (NAM) and the West African monsoon (WAM). However, penetration due to ASM convection is deeper into the UTLS as compared to NAM and WAM outflow. The circulation in these monsoon regions distributes PAN into the tropical latitude belt in the upper troposphere. Remote transport also occurs in the extratropical upper troposphere where westerly winds drive North American and European pollutants eastward to partly merge with the ASM plume. Strong ASM convection transports these remote and regional pollutants into the lower stratosphere. In the lower stratosphere the injected pollutants are transported westward by easterly winds.

The intense convective activity in the monsoon regions is associated with lightning generation and thereby the emission of NO_y species. This will affect the distribution of PAN in the UTLS. The estimates of lightning produced PAN, HNO_3, NO_x and ozone obtained from control and lightning-off simulations shows high percentage changes over the regions of convective transport especially equatorial Africa and America and comparatively less over the ASM. This indicates higher anthropogenic pollution transport from the ASM region into the UTLS.

1 Introduction

Deep monsoon convection plays a key role in venting chemical constituents from the boundary layer and their export from source regions (Dickerson et al., 1987). The largest regional monsoon systems are the North American monsoon (NAM), Asian Summer Monsoon (ASM), Western North Pacific monsoon (WNPM), South American monsoon (SAM), West African Monsoon (WAM), and the Australian Monsoon (AUSM) (Chang et al., 2011). Recent observations and modeling studies indicate that the Asian summer monsoon (Park et al., 2004; Li et al., 2005; Randel and Park, 2006; Fu et al., 2006; Park et al., 2007; Xiong et al., 2009; Randel et al., 2010; Fadnavis et al., 2013), the North American Monsoon (Schmitz and Mullen, 1996; Collier and Zhang, 2006; Barth et al., 2012) and the West African monsoon (Bouarar et al., 2011) play important roles in the transport of chemical constituents out of the boundary layer into the monsoon anticyclone in the upper troposphere and lower stratosphere. Model simulations also suggest that transported pollutants from the Asian monsoon region could contribute substantially to the budgets of stratospheric ozone, NO_x and water vapour (Randel et al., 2010). Transport of ozone precursors rich with VOCs during North American monsoon enhances ozone in the anticyclone (Li et al., 2005; Zhang et al., 2008; Choi et al., 2009; Barth et al., 2012). The deep monsoon convection over West Africa transports Central African emissions to the UTLS leading to large ozone changes in the lower stratosphere (Bouarar et al., 2011). Although a number of papers have reported transport of chemical constituents into the UTLS due to the Asian monsoon convection, less attention has been paid to deep convective transport from North/South America and West Africa to the lower stratosphere and to their relative contributions to the UTLS composition.

Peroxyacetylnitrate (PAN) is formed by the oxidation of non methane volatile organic compounds (NMVOCs) in the presence of NO_x (Fischer et al., 2013). The major sources of NMVOCs are the emissions from fossil fuel and biofuel combustion and from industrial solvents (Tang et al., 2009), while fossil fuel combustion is primary source for

NO_x (Fischer et al., 2013). Biomass burning, natural plant and soil emissions also contribute to NMVOC and NO_x production. In the upper troposphere, lightning can add substantial amounts of NO_x and thus lead to additional PAN production if NMVOC precursors are present, e.g. from convective uplifting from the boundary layer.

The estimated global NO_x production by lightning is ~ 3–$5\,\mathrm{Tg\,N\,year^{-1}}$ (Schumann and Huntrieser, 2007; Martin et al., 2007; Murray et al., 2012). Strong lightning activity during ASM, NAM and WAM (Shepon et al., 2007; Evett et al., 2008; Ranalkar and Chaudhari, 2009; Barret et al., 2010; Penki and Kamra, 2013) contributes to PAN production via lightning NO_x. The estimated increase in PAN is ~ 20–$30\,\%$ due to nitrogen enhancement by lightning (Tie et al., 2001). The main loss reactions of PAN are thermal decomposition (most important in the lower troposphere up to $\sim 500\,\mathrm{hPa}$), photolysis (most important in the UTLS), and the reaction with OH (Talukdar et al., 1995; Fischer et al., 2013).

Due to the cold temperatures in the UTLS, the chemical lifetime of PAN in this region is several months. The PAN lifetime in ECHAM5-HAMMOZ simulations varies between 80 and 200 days in the tropical UTLS (figure not included). PAN therefore travels over long distances and affects the NOy partitioning in areas that are far away from the precursor emission regions. Upon descent into warmer regions of the troposphere, PAN released NO_x increases ozone and OH production in remote regions (Singh et al., 1986, 1998; Hudman et al., 2004). PAN mixing ratios vary from less than 1 pptv in the remote marine atmosphere (as observed during the NASA GTE PEM-Tropics B campaign in the South Pacific lower marine boundary layer, data available at http://acd.ucar.edu/~emmons/DATACOMP/) to several ppbv in the polluted urban environment and biomass burning plumes (Ridley et al., 1992; Singh et al., 1998). In the UTLS mixing ratios are typically in the range 10–300 pptv (Emmons et al., 2000; Keim et al., 2008).

In this paper we analyze the influence of monsoon outflow from different world regions on the distribution of peroxyacetyl nitrate (PAN) in the UTLS. This analysis compares the ECHAM5-HAMMOZ chemistry climate model simulations with data from

aircraft campaigns and the Michelson Interferometer for Passive Atmospheric Sounding (MIPAS) instrument onboard the ENVIronmental SATellite (ENVISAT). The paper is organized as follows: Sect. 2 contains a short description of the data and model including the simulation setup. ECHAM5-HAMMOZ results are evaluated with airborne and MIPAS-E measurements in Sect. 3. In Sect. 4, we discuss the various convective transport pathways of PAN into the UTLS; its redistribution in the stratosphere and recirculation across the various monsoon regions. The analysis of percentage change in lightning produced ozone, HNO_3, PAN and NO_x on total concentration over the convective zones is also presented. Conclusions are given in Sect. 5.

2 Methods

2.1 Satellite measurements

The MIPAS–E instrument onboard the ENVISAT was launched in March 2002 into a polar orbit of 800 km altitude, with an orbital period of about 100 min and an orbit repeat cycle of 35 days. MIPAS-E (Fischer and Oelhaf, 1996; Fischer et al., 2008) was a Fourier Transform Spectrometer that provided continual limb emission measurements in the mid infrared over the range 685–$2410\,\mathrm{cm^{-1}}$ (14.6–4.15 µm). From June 2002 to March 2004 MIPAS-E operated in its full spectral resolution mode at an unapodized resolution of $0.035\,\mathrm{cm^{-1}}$, and with tangent altitude steps of 3 km in the UTLS. From January 2005 through the end of the mission in April 2012 the spectral resolution was reduced to $0.0875\,\mathrm{cm^{-1}}$, while the tangent altitude steps in the UTLS were reduced to 1.5–2 km. MIPAS-E monitored several atmospheric trace constituents affecting atmospheric chemistry including PAN, NO_x, and O_3. The details of the general retrieval method and setup, error estimates and use of averaging kernel and visibility flag are documented by Von Clarmann et al. (2009). Details of the PAN retrievals, error budget, and vertical resolution are given by Glatthor et al. (2007) for 2002–2004, and by Wiegele et al. (2012) for 2005–2012 measurement periods.

In this study we analyze the MIPAS-E observed PAN data during the period 2002–2011. The data are available at http://share.lsdf.kit.edu/imk/asf/sat/mipas-export/Data_by_Target/. The data versions used in this study are V3O_PAN_5 for 2002–2004, and V5R_PAN_220/V5R_PAN_221 for 2005–2011. The data are processed as per the quality specifications given in the documentation. The useful height range is specified as 5 to 23 km. The data are contoured and gridded at 4° longitude and 8° latitude resolution.

2.2 ECHAM5-HAMMOZ model simulation and experimental setup

The ECHAM5-HAMMOZ aerosol–chemistry–climate model used in the present study comprises of the general circulation model ECHAM5 (Roeckner et al., 2003), the tropospheric chemistry module, MOZ (Horowitz et al., 2003), and the aerosol module, Hamburg Aerosol Model (HAM) (Stier et al., 2005). It includes ozone, NO_x, VOC and aerosols chemistry. The gas phase chemistry scheme is based on the MOZART-2 model (Horowitz et al., 2003), which includes comprehensive O_x-NO_x-hydrocarbons chemistry with 63 tracers and 168 reactions. The $O(^1D)$ quenching reaction rates were updated according to Sander et al. (2003), and isoprene nitrates chemistry according to Fiore et al. (2005). The PAN formation process occurs through the reaction of the peroxy acetyl radical (CH_3CO_3) and NO_2. This reaction is reversible and the thermal decomposition of PAN back to CH_3CO_3 and NO_2 is the main sink of PAN. The reaction rates for this reversible reaction are updated in Horowitz et al. (2003). CH_3CO_3 is mainly formed by oxidation of acetaldehyde (CH_3CHO) by OH, and by the photolytic decomposition of acetone (CH_3COCH_3) and methylglyoxal (CH_3COCHO). In the model simulations we included emissions of acetone from anthropogenic sources and wild fires (primary sources), while acetaldehyde and methylglyoxal are produced by oxidation of other NMVOCs (secondary sources). In particular, oxidation of primary NMVOCs like ethane (C_2H_6), propane (C_3H_8) and propene (C_3H_6) forms acetaldehyde, while CH_3COCHO is mainly formed from the oxidation products of isoprene and terpenes. Higher acyl peroxy nitrates (MPAN) are included in MOZART-2 chemical scheme, they

are also formed through oxidation of NMVOCs, but their production is small compared to PAN. In the global mean, the main loss process of PAN from the atmosphere is the thermal decomposition into its precursors. Photolysis and reaction with OH are of relatively minor importance but matter in the UTLS region.

In ECHAM5-HAMMOZ dry deposition follows the scheme of Ganzeveld and Lelieveld (1995). Soluble trace gases such as HNO_3 and SO_2 are also subject to wet deposition. In-cloud and below cloud scavenging follows the scheme described by Stier et al. (2005). PAN is not highly water soluble, therefore dry and wet depositions are insignificant removal process.

The model is run at a spectral resolution of T42 corresponding to about 2.8° × 2.8° in the horizontal dimension and 31 vertical hybrid σ-p levels from the surface up to 10 hPa. The details of model parameterizations, emissions and validation are described by Pozzoli et al. (2008a, b, 2011) and Fadnavis et al. (2013). Our base year for aerosol and trace gas emissions is 2000, and emissions were repeated annually throughout the simulation period except for biogenic VOC, dust and sea salt emissions, which are parameterized according to the meteorology. The simulations were run as AMIP simulations with specified sea surface temperature (SST) and sea ice (SIC) data over the period 1995–2004.

To study the impact of lightning on the distributions of PAN we compare two sets of experiments; each conducted for 10 years 1995–2004: (1) the control experiment (CTRL) and (2) the lightning off experiment (light-off). The parameterization of the lightning emissions is according to Grewe et al. (2001). The mass of atomic nitrogen produced as NO per flash is 9 kg. Lightning diagnostics are output hourly.

3 Results and discussion

3.1 Comparison with aircraft measurements

Model simulated PAN, NO_x, HNO_3 and Ozone mixing ratios are evaluated with climatological datasets of airborne campaigns during the monsoon season (June–September). The data were retrieved from http://acd.ucar.edu/~emmons/DATACOMP/CAMPAIGNS/. The NO_x and ozone volume mixing ratios observed during CAIPEEX experiment, September 2010, are evaluated over the Indian region. The details of instrument and measurement technique are available at http://www.tropmet.res.in/~caipeex/about-data.php. The list of data sets and aircraft campaign used for comparison are presented in Table 1. For the comparison, aircraft observations are averaged over 0–2 km, 2–6 km and 6–8 km and at the center latitude and longitude of the flight region.

Figure 1a–k compares the observed global distribution of PAN, ozone, HNO_3 and NO_x to those simulated by ECHAM5-HAMMOZ. The mean aircraft observations (listed in Table 1) are shown as filled circles and model output are background contours. Figure 1 indicates that model simulated PAN, HNO_3 and NO_x show good agreement with aircraft measurements however model ozone concentrations in the lower troposphere (0–6 km) are higher over South America. In the upper troposphere (6–10 km) model simulated ozone compares better with aircraft observations. Model simulated ozone and NO_x show good agreement with CAIPEEX measurements over the Indian region.

3.2 Comparison with MIPAS-E measurements

In order to study the influence of monsoon circulation on the distribution of PAN in the UTLS region, seasonal mean (June–September) PAN concentrations are analyzed. Figure 2a and b present the seasonal mean distributions of the PAN retrievals from MIPAS-E at 14 and 16 km averaged over the period 2002–2011. Simulated PAN concentrations by ECHAM5-HAMMOZ are plotted in Fig. 2c and d for comparison. Figure 2a shows a maximum in PAN concentrations (~ 200–230 ppt) over the Asian

monsoon anticyclone region (12–40° N, 20–120° E), and over parts of North America, the Gulf Stream, southern Atlantic Ocean and west coast of tropical Africa. ECHAM5-HAMMOZ CTRL simulations also show high PAN concentration at these locations (Fig. 2c), however PAN concentrations are lower than MIPAS-E observations and appear somewhat more localized. At 14 km altitude, MIPAS-E exhibits a PAN maximum originating from African sources over the South Atlantic, whereas the model shows this maximum over the African continent. This may be the outflow of biomass burning over central and southern Africa during summer monsoon which is underestimated in the model. From aircraft observations and model simulations Real et al. (2010) reported a plume in the mid and upper troposphere over southern Atlantic which originates from central African biomass burning fire. These differences may also be related to issues in the vertical transport of PAN, or to a possible underestimate of the emission sources of non methane volatile organic compounds. Uncertainties in the rate coefficients and absorption cross sections of PAN may also play a role. Also anthropogenic emissions are mostly underestimated in the emission inventories (Miyazaki et al., 2012). The comparison of cross-section plots of MIPAS-E PAN with model simulated PAN at various altitudes (8–23 km) indicate that in the UTLS, MIPAS-E PAN is higher than model simulated PAN by ~ 20–60 ppt. It is lower by 20–40 ppt over eastern part of anticyclone and 40–50 ppt over Indonesia and Northern Australia. Near the southern pole MIPAS-E PAN is higher than ECHAM5-HAMMOZ by 70–90 ppt. The model could not produce high PAN concentrations near the southern pole between 17 and 23 km. In the ASM region during the monsoon season MIPAS-E PAN is higher than model by 30–60 ppt. The comparison of PAN measurements from MIPAS-E with Atmospheric Chemistry Experiment-Fourier Transform Spectrometer (ACE-FTS) indicates that MIPAS-E PAN is higher than ACE-FTS in the UTLS by 70 ppt at the altitudes between 9.5–17.5 km, which lies within limits of measurement error (Tereszchuk et al., 2013). This indicates that model simulated PAN concentrations in the UTLS show reasonable agreement with MIPAS-E.

4 Transport pathways

4.1 Transport from northern tropical land mass

From Fig. 2a–d it appears that air pollution is rising from Asia, North America and tropical Africa into the UTLS. Monsoon convective activity over Asia (June–September), North America (July–September) and tropical Africa (June–September, 10° N–25° S) appears to play a dominant role in vertical transport. Some fraction of this convective transport can reach the lower stratosphere (Park et al., 2009) and subsequent horizontal transport can redistribute PAN in the stratosphere.

To illustrate vertical transport, longitude-altitude cross sections of PAN mixing ratios averaged over the ASM anticyclone region (0–30° N) and for June–September as obtained from MIPAS-E and ECHAM5-HAMMOZ at the altitudes 8–23 km are shown in Fig. 3a and b respectively. Both MIPAS-E observations and ECHAM5-HAMMOZ simulations show elevated levels of PAN (200–250 ppt) near 80–100° E (ASM), 30° W-30° E (WAM) and 80–100° W (NAM) regions. The winds plotted in Fig. 3b show cross tropopause transport from these regions. Figure 3c reveals that transport of boundary layer PAN to UTLS mainly occurs from strong convective regions, mainly Bay of Bengal (∼ 80–90° E), South China Sea (∼ 100–120° E), western Atlantic Ocean (Gulf Stream region) and Gulf of Mexico (80–100° W). The transport due to ASM is stronger and reaches deeper into the lower stratosphere. This is due to the more intense deep convection activity over the ASM region compared to the NAM region. The low potential vorticity (PV) area indicate the strength of the monsoon anticyclone (Garny and Randel, 2013). The analysis of model simulated potential vorticity at 370 K, shown in Fig. 4 exhibits lower PV values over the ASM region compared to the NAM region. This reflects a stronger monsoon anticyclone over ASM. Out of all the regions in question convective activity is most intense over the region spanning the Bay of Bengal and the Maritime Continent (e.g. Gettelman et al., 2002; see their Fig. 3). The tropopause temperatures are typically the lowest in this region. Deep convection intensity is significant

over Central America as well but is much more localized and not effective at pumping North American NO_x emissions into the UTLS.

4.2 Transport from southern tropical land mass

In order to understand transport of PAN due to southern WAM, SAM and AUSM, we consider longitude-pressure sections of MIPAS-E observations and model simulated PAN concentrations averaged over 0–25° S. PAN concentrations from MIPAS-E and model simulations are plotted in Fig. 3d and e respectively. The model has plumes near 20° E, 100° E and 80° W which are clearest in the view including the boundary layer PAN distribution is plotted in Fig. 3f. These three regions of convective transport are (1) tropical south Africa 10–40° E, referred as south Africa, (2) Indonesia and northern parts of Australia ∼ 100–110° E and (3) South America ∼ 70–80° W. Outflow from Indonesia and from northern parts of Australia (∼ 100° E) penetrates deeper into the UTLS. Figure 4 shows lower PV values (PV negative in Southern Hemisphere, Dong and Colucci, 2005) over Indonesia and northern part of Australia confirming tropospheric air mass in the lower stratosphere. Tropical Rainfall Measuring Mission (TRMM) satellite observations show high frequency of intense overshooting convection over these areas (during the monsoon season) with highest density in the belt 0–10° S over the Caribbean, Amazon, Congo and Southern Maritime Continent (Liu and Zipser, 2005). The analyses of vertical winds show strong transport from 10–40° E, 100–110° E, 70–80° W (in the belt 0–10° S). The amount of high level cloud fraction is also high over these regions. The model simulations show high PAN concentrations reaching the UTLS. Thus transport due to deep convection is reasonably well captured by the model. However, the MIPAS-E observations only show a plume rising over South Africa, The AUSM (Indonesia-Australia) and SAM plumes are not distinguishable at these altitudes. Figure 3f shows that in the upper troposphere (8–14 km) they are mixed by the prevailing westerly winds. The reasons for a single plume seen in MIPAS-E may be that lower concentrations of PAN reach these altitudes (above 8 km) from SAM and AUSM and mix with plumes over South Africa. Longitude-altitude cross section of model simulation

in the upper troposphere (Fig. 3e) shows less PAN concentrations over the longitudes of SAM and AUSM (see Fig. 3e). It is also possible that the three plume structure in the upper troposphere seen in model is being obscured in the observations due to sampling issues and coarse resolution.

Figure 3a–f shows that simulated transport of PAN due to ASM, NAM and WAM convection are stronger and penetrate deeper into the upper troposphere compared to SAM and AUSM. This is consistent with the distribution of deep convection noted by Gettelman et al. (2002). However, the PAN amounts in the UTLS in the model are less than observed by MIPAS-E. This may be due to an underestimate of the chemical PAN source from VOC precursors or too little vertical transport or a combination of both. Earlier model studies with ECHAM also exhibited too low concentrations of CO in the upper tropospheric outflow (M.G. Schultz, unpublished data from the NASA).

4.3 Transport from Asian Summer Monsoon region

The latitude-altitude sections over the ASM (60–120° E) of MIPAS-E observed PAN (plotted in the altitude range 8–23 km) and ECHAM5-HAMMOZ CTRL simulations are shown in Fig. 5a and b, respectively. ECHAM5-HAMMOZ simulations are similar to MIPAS-E retrievals of PAN. There is indication of plume ascent into the lower stratosphere. The ECHAM5-HAMMOZ simulations also show transport of subtropical boundary layer PAN into the UTLS (see Fig. 5c) due to deep convection. This is not visible in the MIPAS-E data because of the lack of data below 8 km. Figure 5c shows that there is transport from 40–50° N reaching up to 10 km (~ 200 hPa). Park et al. (2004, 2007, 2009) and Randel and Park (2006) noted that trace species are introduced into the monsoon anticyclone at its eastern end around 200 hPa. The uplift over south-east Asia and the base of the Himalayas in India pumps tracers into the upper tropical troposphere where they get horizontally redistributed by the anticyclonic circulation and form the region of high PAN values between 40° N and high latitudes. Figure 7c shows that the mid-latitude maximum seen in Fig. 5c is due to pollution transport from Europe.

The Chinese emissions are feeding into this large plume over Russia and partly being transported and diluted over the extratropical Pacific Ocean.

4.4 Transport from North American monsoon region

Figure 5d and e exhibit latitude-altitude sections of PAN from MIPAS-E retrievals and ECHAM5-HAMMOZ simulations (seasonal mean for July–September) over the North American monsoon region between 70W-120W. MIPAS-E observations and the model indicate transport of PAN into the UTLS. The distribution of ECHAM5-HAMMOZ simulated PAN from the boundary layer to UTLS (see Fig. 5f) shows that the source region is at around 30° N. There is convective uplift of PAN over the northern Gulf of Mexico region and over the Gulf Stream. High amounts of pollutants are emitted from north east America from a number of power plants located in Atlanta, Washington, Chicago, Boston, Jacksonville (CEC report, 2011). The tropospheric NO_2 columns retrieved from the SCIAMACHY and OMI satellite instrument shows high amount of anthropogenic NO_2 emissions over this region (Lamsal et al., 2011; Miyazaki et al., 2012). The Model simulations show high amount of PAN concentrations over this region (Fig. 7a–d). The monsoon convection lifts these pollutants to the upper troposphere. The outflow of these pollutants is over the Atlantic (see Fig. 2a). TRMM precipitation radar observations show significant overshooting convective activity over this region during the monsoon season (Liu and Zipser, 2005).

4.5 Transport from West African region

Figure 5g–i show vertical distributions of PAN over the African region (averaged over 0–45° E). MIPAS-E observations and model simulations indicate a plume that crosses the tropopause and enters the lower stratosphere. The model surface fields (see Fig. 5i) show that this plume arises from latitudes 5–20° S over Africa and that it moves equatorward. It subsequently merges with the ASM plume. A prominent tongue of high PAN values between 30 and 60° N is captured in model simulations. This feature appears to

be related to emissions from Europe being transported towards the equator in the upper subtropical troposphere. However, in the model, emissions from Europe, are transported poleward instead of equatorward (Fig. 5i). There is a region of strong descent in the model between 30 and 40° N (see Fig. 5h) which deforms the PAN isopleths around 12 km around 30° N downward. This feature is not seen in the MIPAS-E retrievals and indicates a disagreement of the model with the transport pattern of the atmosphere in this region. The transport of PAN in the 10–20° S latitude band over the Congo, Angola, Tanzania regions of southern and tropical Africa is not pronounced in the model compared to MIPAS-E observations. This behavior indicates that deep tropical convection is underestimated in the model in this latitude band.

The model simulated latitude-altitude, longitude-altitude cross sections of NO_x, and HNO_3 over the ASM (10–40° N, 60–120° E), NAM (10–40° N, 70–120° W) and WAM (0–25° S, 0–45° E) are shown in Fig. 6 panel a and b. Figure 6 in panel a shows transport features in NO_x. These are similar to those seen in the distribution of PAN. This shows that monsoon convection lifts boundary layer pollutants including NO_y species to the UTLS. The distribution of HNO_3 (shown in Fig. 6 panel b). Comparing with Fig. 3b and c the region around 100° E with intense convective uplift corresponds to HNO_3 depletion from the surface to above 10 km. In fact, the upper troposphere region of the ASM anticyclone exhibits much lower values of HNO_3 compared to all the other longitudes in the 10–40° N band (Fig. 6c in panel b). This suggests that in the model the convective transport in the ASM region is associated with efficient removal by wet scavenging. In contrast, the North American monsoon region has HNO_3 ascending to the upper troposphere with significantly less loss. This is likely due to the fact that convection involved in vertical transport during the NAM is not as intense and not as deep as in the case of the ASM and there are differences in wet scavenging. Figure 6b in panel b shows that the plume rising from South America moves towards the equator but does not have the extension into the upper troposphere as the North American plume. These are June–September averages and the ITCZ is on the Northern Hemisphere side during this period. Thus, weaker convective transport is to be expected on the

Southern Hemisphere side of the equator during this period. Figure 6d in panel b shows significant transport of African emissions around ~ 0–15° S and a plume rising from Europe (~ 35–60° N) as well.

4.6 Horizontal transport

PAN concentrations from MIPAS-E and ECHAM5-HAMMOZ simulations at different altitudes are analyzed to understand horizontal transport. Figure 7a shows distribution of PAN from ECHAM5-HAMMOZ simulations near the surface (1 km). Sources of PAN are apparent over South America, southern Africa, North America, Europe, Russia and northern China/Mongolia. The PAN distribution at 3 km (see Fig. 7b) shows high concentrations above these regions indicating vertical transport. Figure 7c shows the distribution at 6 km. There is transport of PAN from central Africa towards America and from Brazil towards Africa.

The LBA-CLAIRE-98 campaign observations (Andreae et al., 2001) and African Monsoon Multidisciplinary Analysis (AMMA) project (Real et al., 2010) show that the biomass burning plume originating from Brazil is lifted to altitudes around 10 km. This plume is entrained into deep convection over the northern Amazon, transported out over the Atlantic and then returned to South America by the circulation around a large upper-level anticyclone. This transport is well captured by the model.

North American pollution is also being transported by the westerly winds over Eurasia, forming an organized belt. This transport pattern persists up to 12 km (Fig. 7e and g). MIPAS-E observations at 12 km also show this transport pattern. The source region for the PAN from southern Africa is the region of active biomass burning. Since this region is tropical, the outflow is over the Atlantic due to the prevailing easterly zonal winds. ECHAM5-HAMMOZ simulations shows similar transport (see Fig. 7g). But there are differences; in particular the transport over tropical Africa does not get displaced over the Atlantic Ocean. As noted above, there are significant transport differences between the model and observations in this longitude band. Another difference is that PAN is not transported westward over Central America and towards the Pacific Ocean.

Figure 7f–h show the distribution of PAN from MIPAS-E retrievals and ECHAM5-HAMMOZ simulations, in the lower stratosphere (18 km). In both data sets PAN is transported westwards from ASM, NAM and WAM by prevailing easterly winds.

As can be seen from the above discussions, the ASM, NAM, and WAM outflow and convection over the Gulf Stream play an important role in the transport of boundary layer pollution into the UTLS. Previous studies (e.g. Fadnavis et al., 2013) indicate that over the Asian monsoon region, transport into the lower stratosphere occurs and there is significant vertical transport over the southern slopes of the Himalayas (Fu et al., 2006; Fadnavis et al., 2013) and also over the region spanned by the Bay of Bengal and the South China Sea (Park et al., 2009). Pollutant transport due to North American convection and tropical African outflow does not penetrate as deep into the stratosphere as the ASM. However there is clear indication of upper troposphere transport in middle latitude westerly winds that connects North American pollution to the ASM.

Figures 2–5 show that in the upper troposphere, westerly winds drive North American and European pollutants eastward to at least partly merge with the ASM plume. Strong ASM convection transports these remote and regional pollutants into the stratosphere. The Caribbean is a secondary source of pollutant transport into the stratosphere. In the stratosphere the injected pollutants are transported westward by easterly winds and into the southern subtropics by the Brewer–Dobson circulation.

4.7 Impact of lightning on tropospheric PAN, NO_x, HNO_3 and ozone

Long-range transport of PAN may increase NO_x and hence ozone concentrations at remote locations. In the tropical lower troposphere, NO_x is rapidly converted into HNO_3 due to high amounts of OH. During the monsoon season the intense solar radiation along with high background concentrations of NO_x, HO_x and NMVOCs and intense lightning activity can affect the formation and distribution NO_x, PAN, HNO_3 and ozone (Tie et al., 2001). The percentage change in lightning source of ozone, HNO_3, PAN and NO_x on total concentration is computed from the control and lightning-off experiments. Lightning production of NO_x, HNO_3 and ozone may affect PAN concentrations

in the UTLS though heterogeneous reactions. We analyze the spatial distribution of ozone, HNO_3, PAN and NO_x respectively produced from lightning at mid-tropospheric and upper tropospheric pressure levels by plotting the differences between the simulations. Figure 8a–d shows changes in zonally averaged spatial distribution of seasonal mean (June–September) ozone, HNO_3, PAN and NO_x respectively. The analysis indicates that the impact of lightning on these species is high in the tropical upper troposphere. The enhancement takes place between 40° N–40° S and between 8 and 14 km. In the tropical mid troposphere lightning produced maximum ozone is ∼ 15–25 %, HNO_3 ∼ 40–60 % ∼ PAN ∼ 15–25 % and NO_X ∼ 20–40 % while in the upper troposphere ozone is ∼ 20–30 %, HNO_3 ∼ 60–75 %, PAN ∼ 28–35 %, and NO_x ∼ 50–75 %. MOZART model simulations also show that lightning enhances PAN formation by 20–30 %, NO_x ∼ 50 % and HNO_3 by 60–80 % in the middle troposphere (Tie et al., 2001). Labrador et al. (2005) reported similar results from simulations using the Model of Atmospheric Transport and Chemistry Max-Planck-Institute (MATCH-MPI). The spatial distribution of NO_x, ozone, and PAN and HNO_3 produced from lightning (see Fig. 8e–h) indicate that in the upper troposphere (12 km) increase in O_3 ∼ 20–25 % (11–17 ppbv), HNO_3 ∼40–70 %, PAN ∼ 25–35 % and NO_x ∼ 55–75 %, over North America are in agreement with previous studies (e.g Labrador et al., 2005; Hudman et al., 2007; Zhao et al., 2009; Cooper et al., 2009), over equatorial Africa (PAN 30–45 %, HNO_3 ∼ 70–80 %, O_3 ∼ 25 %, NO_x ∼ 70 %) agrees well with Barret et al., 2010; Bouarar et al., 2011 and over the ASM region (PAN ∼ 25 %, HNO_3 ∼ 65–70 %, O_3 ∼ 20 %, NO_x ∼ 60–70 %) agrees with Tie et al. (2001). These regions coincide with regions of convective vertical transport of PAN (as seen in Figs. 3 and 5). They will be lifted into the lower stratosphere by the monsoon convection along with anthropogenic emissions and will redistribute in the tropical lower stratosphere. Latitude-longitude cross sections of lightning produced PAN, NO_x, ozone and HNO_3 at altitudes between 8–14 km show production of PAN, NO_x, ozone and HNO_3 is relatively less over the ASM region than the equatorial Americas and Africa (also seen in Fig. 8). However, the vertical distribution shows high amounts of PAN transported in the upper troposphere from the ASM (see Figs. 2, 3

and 5). This indicates higher amounts anthropogenic emission transport into the UTLS from the ASM.

5 Conclusions

Analysis of PAN observations from the MIPAS instrument on the Envisat satellite for the period 2002–2011 and ECHAM5-HAMMOZ global model simulations shows that during monsoon season pollution outflow from Asian summer monsoon (ASM), North American Monsoon (NAM) and West African monsoon (WAM) regions penetrates into the UTLS. However, penetration due to ASM convection is deeper than in the NAM and WAM regions during the June–September period and partly extends into the stratosphere. In the upper troposphere, westerly winds drive North American and northward propagating South African pollutants eastward and they mix with the ASM plume. Deep, overshooting convection and strong diabatic upwelling in the ASM region convection transports a part of these plumes into the lower stratosphere. Some cross tropopause transport occurs due to overshooting convection over North America and Southern Africa as well (Khaykin et al., 2009; Randel et al., 2012; Hassim et al., 2014). In the lower stratosphere the injected pollutants from ASM, WAM and NAM are transported westward by easterly winds and into the Southern Hemisphere subtropics by the Brewer–Dobson circulation. In the Southern Hemisphere, plumes rising from convective zones of South Africa, South America and Indonesia-Australia are evident in model simulations. PAN concentrations are higher in the plume rising from South Africa than SAM and AUSM. In the upper troposphere, they merge by the prevailing westerly winds. MIPAS-E observations in the UTLS show a single plume over South Africa. The reasons for the single plume seen in MIPAS-E may be that lower concentrations of PAN reach these altitudes (above 8 km) from SAM and AUSM and mixing with South African plume. It is also possible that the three plume structure in the upper troposphere seen in the model is being obscured in the observations due to sampling issues and coarse resolution. The horizontal transport of PAN analyzed from ECHAM5–HAMMOZ

simulations shows that the PAN from southern Africa and Brazil is transported towards America by the circulation around a large upper-level anticyclone and then lifted to the UTLS in the NAM region.

Lightning production of NO_y species may enhance PAN concentrations in the upper troposphere and affect its transport in the lower Stratosphere. The percentage change in lightning produced ozone, HNO_3, PAN and NO_x on total concentration has been evaluated using the ECHAM-HAM model. In the upper troposphere, lightning causes significant increases in these species over the equatorial America (PAN ~ 25–35 %, HNO_3 ~ 50–75 %, O_3 ~ 20–25 %, NO_x ~ 55–75 %), equatorial Africa (PAN ~ 30–45 %, HNO_3 ~ 70–80 %, O_3 ~ 25 %, NO_x ~ 70 %) and the ASM region (PAN ~ 25 %, HNO_3 ~ 65–70 %, O_3 ~ 20 %, NO_x ~ 60 %). These regions coincide with intense convective zones with significant vertical transport. Lighting production is higher over equatorial Africa and America compared to the ASM. However, the vertical distribution shows that higher amounts of PAN are transported into the upper troposphere in the ASM region. This indicates higher amount anthropogenic emission transport into the UTLS from the ASM region. This is consistent with the fact that anthropogenic emissions in the ASM region are higher than in the NAM and WAM (Lamsal et al., 2011; Miyazak et al., 2012).

Recent observations show a positive trend (with time) in lightning (Price and Asfur, 2006) and deep convective activity over the tropical land mass (Aumann and Ruzmaikin, 2013). TRMM precipitation radar also shows high density of deep over shooting events over the convective regions of Caribbean, Mexico, Sahara desert, Congo and Indonesia (Liu and Zipser, 2005) during summer monsoon season. This should amplify the UTLS trend from increasing tropospheric pollution. However, an analysis of this process is beyond the scope of this study.

Acknowledgements. The authors thank the MIPAS-E teams for providing data and the High Power Computing Centre (HPC) in IITM, Pune, India, for providing computer resources. S. Fadnavis acknowledges with gratitude B. N. Goswami, Director of IITM, for his encouragement during the course of this study.

References

Andreae, M. O., Artaxo, P., Fischer, H., Freitas, S. R., Grégoire, J.-M., Hansel, A., Hoor, P., Kormann, R., Krejci, R., Lange, L., Lelieveld, J., Lindinger, W., Longo, K., Peters, W., de Reus, M., Scheeren, B., Silva Dias, M. A. F., Ström, J., Velthoven, P. F. J. van and William, J.: Transport of biomass burning smoke to the upper troposphere by deep convection in the equatorial region, Geophys. Res. Lett., 28, 951–958, 2001.

Aumann, H. H. and Ruzmaikin, A.: Frequency of deep convective clouds in the tropical zone from 10 years of AIRS data, Atmos. Chem. Phys., 13, 10795–10806, doi:10.5194/acp-13-10795-2013, 2013.

Barret, B., Williams, J. E., Bouarar, I., Yang, X., Josse, B., Law, K., Pham, M., Le Flochmoën, E., Liousse, C., Peuch, V. H., Carver, G. D., Pyle, J. A., Sauvage, B., van Velthoven, P., Schlager, H., Mari, C., and Cammas, J.-P.: Impact of West African Monsoon convective transport and lightning NO_x production upon the upper tropospheric composition: a multi-model study, Atmos. Chem. Phys., 10, 5719–5738, doi:10.5194/acp-10-5719-2010, 2010.

Barth, M. C., Lee, J., Hodzic, A., Pfister, G., Skamarock, W. C., Worden, J., Wong, J., and Noone, D.: Thunderstorms and upper troposphere chemistry during the early stages of the 2006 North American Monsoon, Atmos. Chem. Phys., 12, 11003–11026, doi:10.5194/acp-12-11003-2012, 2012.

Bouarar, I., Law, K. S., Pham, M., Liousse, C., Schlager, H., Hamburger, T., Reeves, C. E., Cammas, J.-P., Nédélec, P., Szopa, S., Ravegnani, F., Viciani, S., D'Amato, F., Ulanovsky, A., and Richter, A.: Emission sources contributing to tropospheric ozone over Equatorial Africa during the summer monsoon, Atmos. Chem. Phys., 11, 13395–13419, doi:10.5194/acp-11-13395-2011, 2011.

CEC (Commission for Environmental Cooperation): Report on North American Power Plant Air Emissions, Montréal, Canada, 2011.

Chang Yihui Ding , C.-P., Lau, N.-C., Johnson, R. H., Wang, B., and Yasunari, T. (Eds.): The Global Monsoon System: Research and Forecast, 2nd Edn., World Scientific Publishing Co, Singapore, 2011.

Choi, Y., Kim, J., Eldering, A., Osterman, G., Yung, Y. L., Gu, Y., and Liou, K. N.: Lightning and anthropogenic NO_x sources over the United States and the western North Atlantic Ocean: impact on OLR and radiative effects, Geophys. Res. Lett., 36, L17806, doi:10.1029/2009GL039381, 2009.

Collier, J. C. and Zhang, G. J.: Simulation of the North American Monsoon by the NCAR CCM3 and its sensitivity to convection parameterization, J. Climate, 19, 2851–2866, 2006.

Cooper, O. R., Eckhardt, S., Crawford, J. H., Brown, C. C., Cohen, R. C., Bertram, T. H., Wooldridge, P., Perring, A., Brune, W. H., Ren, X., Brunner, D., and Baughcum, S. L.: Summertime buildup and decay of lightning NO_x and aged thunderstorm outflow above North America, J. Geophys. Res., 114, D01101, doi:10.1029/2008JD010293, 2009.

Dickerson, R. R., Huffman, G. J., Luke, W. T., Nunnermacker, L. J., Pickering, K. E., Leslie, A., Lindsey, C., Slinn, W., Kelly, T., Daum, P., Delany, A., Grennberg, J., Zimmerman, P., Boatman, J., Ray, J., and Stedman, D.: Thunderstorms: an important mechanism in the transport of air pollutants, Science, 235, 460–465, 1987.

Dong, L. and Colucci, S. J.: The role of deformation and potential vorticity in Southern Hemisphere blocking onsets, J. Atmos. Sci., 62, 4043–4056, 2005.

Emmons, L. K., Hauglustaine, D. A., Muller, J.-F., Carroll, M. A., Brasseur, G. P., Brunner, D., Staehelin, J., Thouret, V., and Marenco, A.: Data composites of tropospheric ozone and its precursors from aircraft measurements, J. Geophys. Res., 105, 20497–20538, 2000.

Evett, R. R., Mohrle, C. R., Hall, B. L., Brownb, T. J., and Stephens, S. L.: The effect of monsoonal atmospheric moisture on lightning fire ignitions in southwestern North America, Agr. Forest Meteorol., 148, 1478–1487, 2008.

Fadnavis, S., Semeniuk, K., Pozzoli, L., Schultz, M. G., Ghude, S. D., Das, S., and Kakatkar, R.: Transport of aerosols into the UTLS and their impact on the Asian monsoon region as seen in a global model simulation, Atmos. Chem. Phys., 13, 8771–8786, doi:10.5194/acp-13-8771-2013, 2013.

Fiore, A. M., Horowitz, L. W., Purves, D. W., Levy II, H., Evans, M. J., Wang, Y., Li, Q., and Yantosca, R. M.: Evaluating the contribution of changes in isoprene emissions to surface ozone trends over the eastern United States, J. Geophys. Res., 110, D12303, doi:10.1029/2004JD005485, 2005.

Fischer, E. V., Jacob, D. J., Yantosca, R. M., Sulprizio, M. P., Millet, D. B., Mao, J., Paulot, F., Singh, H. B., Roiger, A., Ries, L., Talbot, R.W., Dzepina, K., and Pandey Deolal, S.: Atmospheric peroxyacetyl nitrate (PAN): a global budget and source attribution, Atmos. Chem. Phys., 14, 2679–2698, doi:10.5194/acp-14-2679-2014, 2014.

Fischer, H. and Oelhaf, H.: Remote sensing of vertical profiles of atmospheric trace constituents with MIPAS limb-emission spectrometers, Appl. Optics, 35, 2787–2796, 1996.

Fischer, H., Birk, M., Blom, C., Carli, B., Carlotti, M., von Clarmann, T., Delbouille, L., Dudhia, A., Ehhalt, D., Endemann, M., Flaud, J. M., Gessner, R., Kleinert, A., Koopman, R., Langen, J., López-Puertas, M., Mosner, P., Nett, H., Oelhaf, H., Perron, G., Remedios, J., Ridolfi, M., Stiller, G., and Zander, R.: MIPAS: an instrument for atmospheric and climate research, Atmos. Chem. Phys., 8, 2151–2188, doi:10.5194/acp-8-2151-2008, 2008.

Fu, R., Hu, Y., Wright, J. S., Jiang, J. H., Dickinson, R. E., Chen, M., Filipiak, M., Read, W. G., Waters, J. W., and Wu, D. L.: Short circuit of water vapour and polluted air to the global stratosphere by convective transport over the Tibetan Plateau, P. Natl. Acad. Sci. USA, 103, 5664–5669, 2006.

Ganzeveld, L. and Lelieveld, J.: Dry deposition parameterization in a chemistry general circulation model and its influence on the distribution of reactive trace gases, J. Geophys. Res., 100, 20999–21012, doi:10.1029/95JD02266, 1995.

Garny, H. and Randel, W. J.: Dynamic variability of the Asian monsoon anticyclone observed in potential vorticity and correlations with tracer distributions, J. Geophys. Res.-Atmos., 118, 13421–13433, doi:10.1002/2013JD020908, 2013.

Gettelman, A., Salby, M. L., and Sassi, F.: Distribution and influence of convection in the tropical tropopause region, J. Geophys. Res., 107, 4080, doi:10.1029/2001JD001048, 2002.

Glatthor, N., von Clarmann, T., Fischer, H., Funke, B., Grabowski, U., Höpfner, M., Kellmann, S., Kiefer, M., Linden, A., Milz, M., Steck, T., and Stiller, G. P.: Global peroxyacetyl nitrate (PAN) retrieval in the upper troposphere from limb emission spectra of the Michelson Interferometer for Passive Atmospheric Sounding (MIPAS), Atmos. Chem. Phys., 7, 2775–2787, doi:10.5194/acp-7-2775-2007, 2007.

Grewe, V., Brunner, D., Dameris, M., Grenfell, J. L., Hein, R., Shindell, D., and Staehelin, J.: Origin and variability of upper tropospheric nitrogen oxides and ozone at northern mid-latitudes, Atmos. Environ., 35, 3421–3433, 2001.

Hassim, M. E. E., Lane, T. P., and May, P. T.: Ground-based observations of overshooting convection during the Tropical Warm Pool-International Cloud Experiment, J. Geophys. Res.-Atmos., 119, 880–905, doi:10.1002/2013JD020673, 2014.

Horowitz, L. W., Walters, S., Mauzerall, D. L., Emmons, L. K., Rasch, P. J., Granier, C., Tie, X., Lamarque, J., Schultz, M. G., Tyndall, G. S., Orlando, J. J., and Brasseur, G. P.: A global simulation of tropospheric ozone and related tracers, Description and evaluation of MOZART, version 2, J. Geophys. Res., 108, 4784, doi:10.1029/2002JD002853, 2003.

Hudman, R. C., Jacob, D. J., Cooper, O. R., Evans, M. J., Heald, C. L., Park, R. J., Fehsenfeld, F., Flocke, F., Holloway, J., Hübler, G., Kita, K., Koike, M., Kondo, Y., Neuman, A., Nowak, J., Oltmans, S., Parrish, D., Roberts, J. M., and Ryerson, T.: Ozone production in transpacific Asian pollution plumes and implica tions for ozone air quality in California, J. Geophys. Res., 109, D23S10, doi:10.1029/2004jd004974, 2004.

Hudman, R. C., Jacob, D. J., Turquety, S., Leibensperger, E. M., Murray, L. T., Wu, S., Gilliland, A. B., Avery, M., Bertram, T. H., Brune, W., Cohen, R. C., Dibb, J. E., Flocke, F. M., Fried, A., Holloway, J., Neuman, J. A., Orville, R., Perring, A., Ren, X., Ryerson, T. B., Sachse, G. W., Singh, H. B., Swanson, A., and Wooldridge, P. J.: Surface and lightning sources of nitrogen oxides over the United States: magnitudes, chemical evolution, and outflow, J. Geophys. Res., 112, D12S05, doi:10.1029/2006JD007912, 2007.

Keim, C., Liu, G. Y., Blom, C. E., Fischer, H., Gulde, T., Höpfner, M., Piesch, C., Ravegnani, F., Roiger, A., Schlager, H., and Sitnikov, N.: Vertical profile of peroxyacetyl nitrate (PAN) from MIPAS-STR measurements over Brazil in February 2005 and its contribution to tropical UT NO_y partitioning, Atmos. Chem. Phys., 8, 4891–4902, doi:10.5194/acp-8-4891-2008, 2008.

Khaykin, S., Pommereau, J.-P., Korshunov, L., Yushkov, V., Nielsen, J., Larsen, N., Christensen, T., Garnier, A., Lukyanov, A., and Williams, E.: Hydration of the lower stratosphere by ice crystal geysers over land convective systems, Atmos. Chem. Phys., 9, 2275–2287, doi:10.5194/acp-9-2275-2009, 2009.

Labrador, L. J., von Kuhlmann, R., and Lawrence, M. G.: The effects of lightning-produced NO_x and its vertical distribution on atmospheric chemistry: sensitivity simulations with MATCH-MPIC, Atmos. Chem. Phys., 5, 1815–1834, doi:10.5194/acp-5-1815-2005, 2005.

Lamsal, L. N., Martin, R. V., Padmanabhan, A., van Donkelaar, A., Zhang, Q., Sioris, C. E., Chance, K., Kurosu, T. P., and Newchurch, M. J.: Application of satellite observations for timely updates to global anthropogenic NO_x emission inventories, Geophys. Res. Lett., 38, L05810, doi:10.1029/2010GL046476, 2011.

Li, Q., Jiang, J. H., Wu, D. L., Read, W. G., Livesey, N. J., Waters, J. W., Zhang, Y., Wang, B., Filipiak, M. J., Davis, C. P., Turquety, S., Wu, S., Park, R. J., Yantosca, R. M., and Jacob, D. J.: Convective outflow of South Asian pollution: a global CTM simulation compared with EOS MLS observations, Geophys. Res. Lett., 32, L14826, doi:10.1029/2005GL022762, 2005.

Liu, C. and Zipser, E. J.: Global distribution of convection penetrating the tropical tropopause, J. Geophys. Res., 110, D23104, doi:10.1029/2005JD006063, 2005.

Martin, R. V., Sauvage, B., Folkins, I., Sioris, C. E., Boone, C., Bernath, P., and Ziemke, J.: Space-based constraints on the production of nitric oxide by lightning, J. Geophys. Res., 112, D09309, doi:10.1029/2006JD007831, 2007.

Miyazaki, K., Eskes, H. J., and Sudo, K.: Global NO_x emission estimates derived from an assimilation of OMI tropospheric NO_2 columns, Atmos. Chem. Phys., 12, 2263–2288, doi:10.5194/acp-12-2263-2012, 2012.

Murray, L. T., Jacob, D. J., Logan, J. A., Hudman, R. C., and Koshak, W. J.: Optimized regional and interannual variability of lightning in a global chemical transport model constrained by LIS/OTD satellite data, J. Geophys. Res., 117, D20307, doi:10.1029/2012JD017934, 2012.

Park, M., Randel, W. J., Kinnison, D. E., Garcia, R. R., and Choi, W.: Seasonal variation of methane, water vapour, and nitrogen oxides near the tropopause: satellite observations and model simulations, J. Geophys. Res., doi:10.1029/2003JD003706, 109, D03302, 2004.

Park, M., Randel, W. J., Getteleman, A., Massie, S. T., and Jiang, J. H.: Transport above the Asian summer monsoon anticyclone inferred from Aura Microwave Limb Sounder tracers, J. Geophys. Res., 112, D16309, doi:10.1029/2006JD008294, 2007.

Park, M., Randel, W. J., Emmons, L. K., and Livesey, N. J.: Transport pathways of carbon monoxide in the Asian summer monsoon diagnosed from Model of Ozone and Related Tracers (MOZART), J. Geophys. Res., 114, D08303, doi:10.1029/2008JD010621, 2009.

Penki, R. K. and Kamra, A. K.: Lightning distribution with respect to the monsoon trough position during the Indian summer monsoon season, J. Geophys. Res., 118, 4780–4787, doi:10.1002/jgrd.50382, 2013.

Pozzoli, L., Bey, I., Rast, J. S., Schultz, M. G., Stier, P., and Feichter, J.: Trace gas and aerosol interactions in the fully coupled model of aerosol–chemistry–climate ECHAM5–HAMMOZ: 1. Model description and insights from the spring 2001 TRACE-P experiment, J. Geophys. Res., 113, D07308, doi:10.1029/2007JD009007, 2008a.

Pozzoli, L., Bey, I., Rast, J. S., Schultz, M. G., Stier, P., and Feichter, J.: Trace gas and aerosol interactions in the fully coupled model of aerosol-chemistry-climate ECHAM5–HAMMOZ: 2. Impact of heterogeneous chemistry on the global aerosol distributions, J. Geophys. Res., 113, D07309, doi:10.1029/2007JD009008, 2008b.

Pozzoli, L., Janssens-Maenhout, G., Diehl, T., Bey, I., Schultz, M. G., Feichter, J., Vignati, E., and Dentener, F.: Re-analysis of tropospheric sulfate aerosol and ozone for the period 1980–2005 using the aerosol-chemistry-climate model ECHAM5-HAMMOZ, Atmos. Chem. Phys., 11, 9563–9594, doi:10.5194/acp-11-9563-2011, 2011.

Price, C. and Asfur, M.: Inferred long term trends in lightning activity over Africa, Earth Planets Space, 58, 1197–1201, 2006.

Ranalkar, M. R. and Chaudhari, H. S.: Seasonal variation of lightning activity over the Indian subcontinent, Meteorol. Atmos. Phys., 104, 125–134, 2009.

Randel, W. J. and Park, M.: Deep convective influence on the Asian summer monsoon anticyclone and associated tracer variability observed with Atmospheric Infrared Sounder (AIRS), J. Geophys. Res., 111, D12314, doi:10.1029/2005JD006490, 2006.

Randel, W. J., Park, M., Emmons, L., Kinnison, D., Bernath, P., Walker, K. A., Boone, C., and Pumphrey, H.: Asian monsoon transport of pollution to the stratosphere, Science, 328, 611–613, 2010.

Randel, W. J., Moyer, E., Park, M., Jensen, E., Bernath, P., Walker, K., and Boone, C.: Global variations of HDO and HDO/H_2O ratios in the upper troposphere and lower stratosphere derived from ACE-FTS satellite measurements, J. Geophys. Res., 117, D06303, doi:10.1029/2011JD016632, 2012.

Real, E., Orlandi, E., Law, K. S., Fierli, F., Josset, D., Cairo, F., Schlager, H., Borrmann, S., Kunkel, D., Volk, C. M., McQuaid, J. B., Stewart, D. J., Lee, J., Lewis, A. C., Hopkins, J. R., Ravegnani, F., Ulanovski, A., and Liousse, C.: Cross-hemispheric transport of central African biomass burning pollutants: implications for downwind ozone production, Atmos. Chem. Phys., 10, 3027–3046, doi:10.5194/acp-10-3027-2010, 2010.

Ridley, B. A., Madronich, S., Chatfield, R. B., Walega, J. G., Shetter, R. E., Carroll, M. A., and Montzka, D. D.: Measurements and model simulations of the photostationary state during the Mauna Loa Observatory Photochemistry Experiment: implications for radical concentrations and ozone production and loss rates, J. Geophys. Res., 97, 10375–10388, doi:10.1029/91JD02287, 1992.

Roeckner, E., Bauml, G., Bonaventura, L., Brokopf, R., Esch, M., Giorgetta, M., Hagemann, S., Kirchner, I., Kornblueh, L., Manzini, E., Rhodin, A., Schlese, U., Schulzweida, U., and Tompkins, A.: The Atmospehric General Circulation Model ECHAM5: Part 1, Tech. Rep. 349, Max Planck Institute for Meteorology, Hamburg, 2003.

Sander, S. P., Ravishankara, A. R., Golden, D. M., Kolb, C. E., Kurylo, M. J., Huie, R. E., Orkin, V. L., Molina, M. J., Moortgat, G. K., and Finlayson-Pitts, B. J.: Chemical kinetics and photochemical data for use in atmospheric studies, JPL Publ. 02-25, NASA Jet Propul. Lab., Pasadena, California, 2003.

Schmitz, J. T. and Mullen, S. L.: Water vapor transport associated with the summertime North American Monsoon as depicted by ECMWF analyses, J. Climate, 9, 1621–1634, 1996.
Schumann, U. and Huntrieser, H.: The global lightning-induced nitrogen oxides source, Atmos. Chem. Phys., 7, 3823–3907, doi:10.5194/acp-7-3823-2007, 2007.
Shepon, A., Gildor, H., Labrador, L. J., Butler, T., Ganzeveld, L. N., and Lawrence, M. G.: Global reactive nitrogen deposition from lightning NO_x, J. Geophys. Res., 112, D06304, doi:10.1029/2006JD007458, 2007.
Singh, H. B., Salas, L. J., and Viezee, W.: Global distribution of peroxyacetyl nitrate, Nature, 321, 588–91, 1986.
Singh, H. B., Viezee, W., Chen, Y., Thakur, A. N., Kondo, Y., Talbot, R. W., Gregory, G. L., Sachse, G. W., Blake, D. R., Bradshaw, J. D., Wang, Y., and Jacob, D. J.: Latitudinal distribution of reactive nitrogen in the free troposphere over the Pacific Ocean in late winter/early spring, J. Geophys. Res., 103, 28237–28246, doi:10.1029/98JD01891, 1998.
Stier, P., Feichter, J., Kinne, S., Kloster, S., Vignati, E., Wilson, J., Ganzeveld, L., Tegen, I., Werner, M., Balkanski, Y., Schulz, M., Boucher, O., Minikin, A., and Petzold, A.: The aerosol-climate model ECHAM5-HAM, Atmos. Chem. Phys., 5, 1125–1156, doi:10.5194/acp-5-1125-2005, 2005.
Talukdar, R. K., Burkholder, J. B., Schmoltner, A., Roberts, J. M., Wilson, R. R., and Ravishankara, A. R.: Investigation of loss processes for peroxyacetyl nitrate in the atmosphere: UV photolysis and reaction with OH, J. Geophys. Res., 100, 14163–14173, 1995.
Tang, J. H., Chan, L. Y., Chang, C. C., Liu, S., and Li, Y. S.: Characteristics and sources of non-methane hydrocarbons in background atmospheres of eastern, southwestern, and southern China, J. Geophys. Res., 114, D03304, doi:10.1029/2008JD010333, 2009.
Tereszchuk, K. A., Moore, D. P., Harrison, J. J., Boone, C. D., Park, M., Remedios, J. J., Randel, W. J., and Bernath, P. F.: Observations of peroxyacetyl nitrate (PAN) in the upper troposphere by the Atmospheric Chemistry Experiment-Fourier Transform Spectrometer (ACE-FTS), Atmos. Chem. Phys., 13, 5601–5613, doi:10.5194/acp-13-5601-2013, 2013.
Tie, X. X., Zhang, R., Brasseur, G., Emmons, L., and Lei, W.: Effects of lightning on reactive nitrogen and nitrogen reservoir species in the troposphere, J. Geophys. Res.-Atmos., 106, 3167–3178, doi:10.1029/2000JD900565, 2001.
von Clarmann, T., Höpfner, M., Kellmann, S., Linden, A., Chauhan, S., Funke, B., Grabowski, U., Glatthor, N., Kiefer, M., Schieferdecker, T., Stiller, G. P., and Versick, S.: Retrieval of temperature, H_2O, O_3, HNO_3, CH_4, N_2O, $ClONO_2$ and ClO from MIPAS reduced resolution nominal

mode limb emission measurements, Atmos. Meas. Tech., 2, 159–175, doi:10.5194/amt-2-159-2009, 2009.
Wiegele, A., Glatthor, N., Höpfner, M., Grabowski, U., Kellmann, S., Linden, A., Stiller, G., and von Clarmann, T.: Global distributions of C_2H_6, C_2H_2, HCN, and PAN retrieved from MIPAS reduced spectral resolution measurements, Atmos. Meas. Tech., 5, 723–734, doi:10.5194/amt-5-723-2012, 2012.
Xiong, X., Houweling, S., Wei, J., Maddy, E., Sun, F., and Barnet, C.: Methane plume over south Asia during the monsoon season: satellite observation and model simulation, Atmos. Chem. Phys., 9, 783–794, doi:10.5194/acp-9-783-2009, 2009.
Zhang, L., Jacob, D. J., Boersma, K. F., Jaffe, D. A., Olson, J. R., Bowman, K. W., Worden, J. R., Thompson, A. M., Avery, M. A., Cohen, R. C., Dibb, J. E., Flock, F. M., Fuelberg, H. E., Huey, L. G., McMillan, W. W., Singh, H. B., and Weinheimer, A. J.: Transpacific transport of ozone pollution and the effect of recent Asian emission increases on air quality in North America: an integrated analysis using satellite, aircraft, ozonesonde, and surface observations, Atmos. Chem. Phys., 8, 6117–6136, doi:10.5194/acp-8-6117-2008, 2008.
Zhao, C., Wang, Y., Choi, Y., and Zeng, T.: Summertime impact of convective transport and lightning NO_x production over North America: modeling dependence on meteorological simulations, Atmos. Chem. Phys., 9, 4315–4327, doi:10.5194/acp-9-4315-2009, 2009.

Table 1. Global aircraft measurements used for model evaluation.

Experiment	Date Frame	Species	Location
POLINAT-2 (Falcon)	19 Sep–25 Oct 1997	O_3, NO_x	Canary-Islands: LAT = 25.,35. LON = 340.,350. E-Atlantic: LAT = 35., 45. LON = 330.,340. Europe: LAT = 45.,55. LON = 5.,15. Ireland: LAT = 50.,60. LON = 345.,355.
PEM-Tropics-A (DC8)	24 Aug–15 Oct 1996	O_3, NO_x, HNO_3, PAN	Christmas-Island: LAT = 0.,10. LON = 200.,220. Easter-Island: LAT = −40.,−20. LON = 240.,260. Fiji: LAT = −30.,−10. LON = 170.,190. Hawaii: LAT = 10.,30. LON = 190.,210. Tahiti: LAT = −20.,0. LON = 200.,230.
PEM-Tropics-A (P3)	15 Aug–26 Sep 1996	O_3, HNO_3	Christmas-Island: LAT=0.,10. LON = 200.,220. Easter-Island: LAT = −40.,−20. LON = 240.,260. Hawaii: LAT = 10.,30. LON = 190.,210. Tahiti: LAT = −20.,0. LON = 200.,230.
ABLE-3B (Electra)	6 Jul–15 Aug 1990	O_3, NO_x, HNO_3, PAN	Labrador: LAT = 50.,55. LON = 300.,315. Ontario: LAT = 45.,60. LON = 270.,280. US-E-Coast: LAT = 35.,45. LON = 280.,290.
CITE-3 (Electra)	22 Aug–29 Sep 1989	O_3, NO_x	Natal: LAT = −15.,5. LON = 325.,335. Wallops: LAT = 30.,40. LON = 280.,290.
ELCHEM (Sabreliner)	27 Jul–22 Aug 1989	O_3, NO_x	New-Mexico: LAT = 30.,35. LON = 250.,255.
ABLE-3A (Electra)	7 Jul–17 Aug 1988	O_3, NO_x,PAN	Alaska: LAT = 55.,75. LON = 190.,205.
ABLE-2A (Electra)	12 Jul–13 Aug 1985	O_3	E-Brazil: LAT = −10.,0. LON = 300.,315. W-Brazil: LAT = −5.,0. LON = 290.,300.
STRATOZ-3 (Caravelle 116)	4–26 Jun 1984	O_3	Brazil: LAT = −20.,0. LON = 315.,335. Canary-Islands: LAT = 20.,35. LON = 340.,355. E-Tropical-N-Atlantic: LAT = 0.,20. LON = 330.,345. England: LAT = 45.,60. LON = −10.,5. Goose-Bay: LAT = 45.,60. LON = 290.,305. Greenland: LAT = 60.,70. LON = 290.,330. Iceland: LAT = 60.,70. LON = 330.,355. NW-South-America: LAT = −5.,10. LON = 275.,295. Puerto-Rico: LAT = 10.,25. LON = 290.,300. S-South-America: LAT = −65.,−45. LON = 275.,300. SE-South-America: LAT = −45.,−20. LON = 295.,320. SW-South-America: LAT = −45.,−25. LON = 285.,292. Spain: LAT = 35.,45. LON = −15.,0. W-Africa: LAT = 0.,15. LON = −15.,0. W-South-America: LAT = −25.,−5. LON = 275.,290. Western-N-Atlantic: LAT = 25.,45. LON = 290.,300.
CITE-2 (Electra)	11 Aug–5 Sep 1986	O_3, NO_x, HNO_3, PAN	Calif: LAT = 35.,45. LON=235.,250. Pacific: LAT = 30.,45. LON = 225.,235.
CAIPEEX	Sep 2010 12029	O_3, NO_x	Lat = 17° N, Lon = 73° E

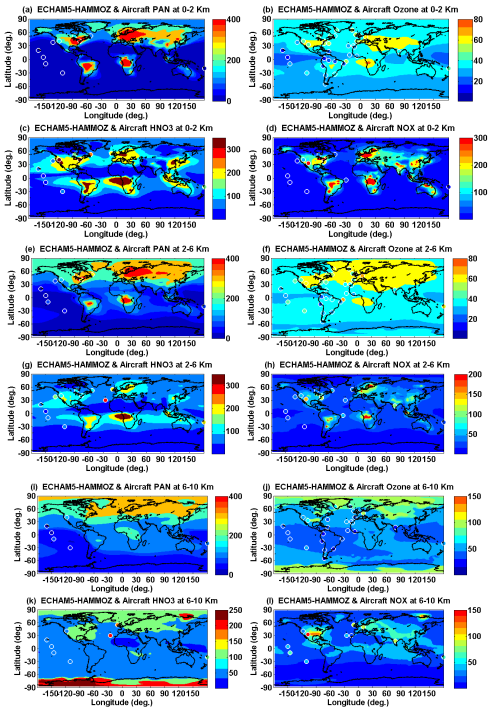

Figure 1. Global mean distribution of PAN (ppt), ozone (ppb), HNO_3 (ppt) and NO_x (ppt) averaged for the monsoon season and altitude ranges. Model results for 1995–2004 (background solid contours) are compared to observations from Table 1 for all years (filled circles). Aircraft observations are averaged vertically and horizontally over the fight region.

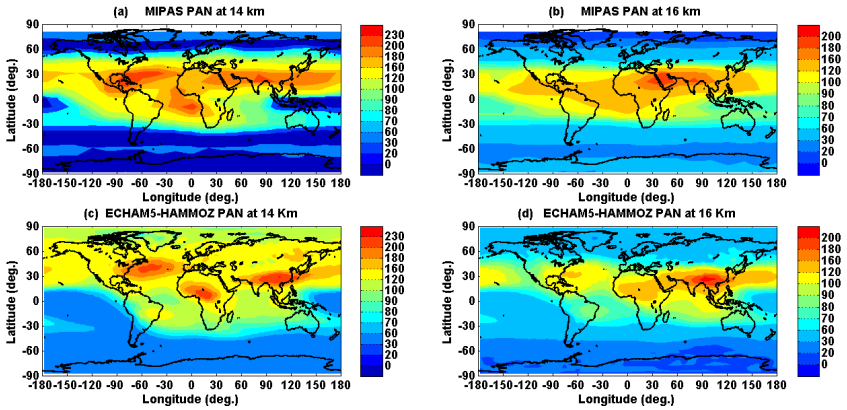

Figure 2. Distribution of seasonal mean PAN concentration (ppt) as observed by MIPAS-E (climatology for the period 2002–2011) at **(a)** 14 km **(b)** 16 km and ECHAM5-HAMMOZ CTRL simulations at **(c)** 14 km **(d)** 16 km. ECHAM5-HAMMOZ simulations are smoothed with averaging kernel of MIPAS-E.

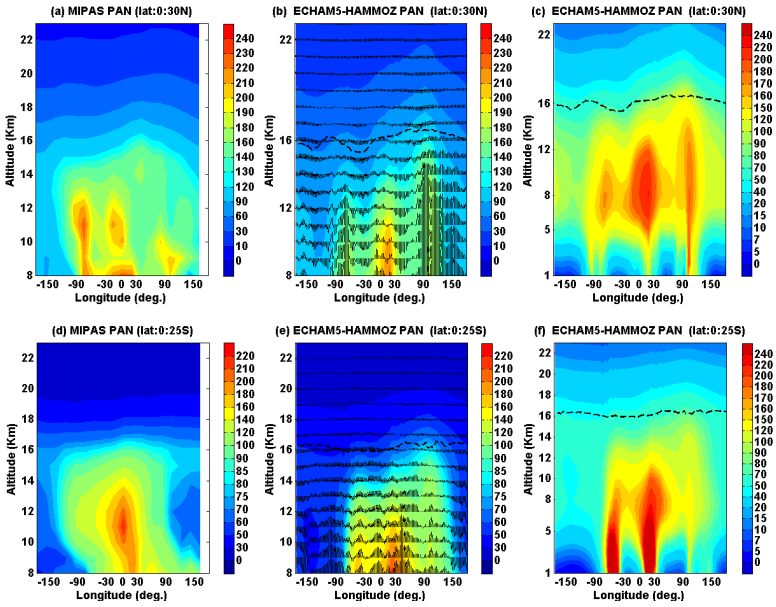

Figure 3. Longitude-altitude cross section of PAN (ppt) averaged for monsoon season and 10–30° N **(a)** MIPAS-E climatology **(b)** ECHAM5-HAMMOZ CTRL simulations between 8–23 km. **(c)** same as figure **(b)** but from the surface. PAN (ppt) averaged for monsoon season and 0–25° S **(d)** MIPAS-E climatology **(e)** ECHAM5-HAMMOZ CTRL simulations between 8–23 km **(f)** same as figure **(e)** but from the surface. ECHAM5-HAMMOZ simulations are smoothed with averaging kernel of MIPAS-E. Wind vectors are indicated by black arrows in figures **(b)** and **(e)**. The vertical velocity field has been scaled by 300.

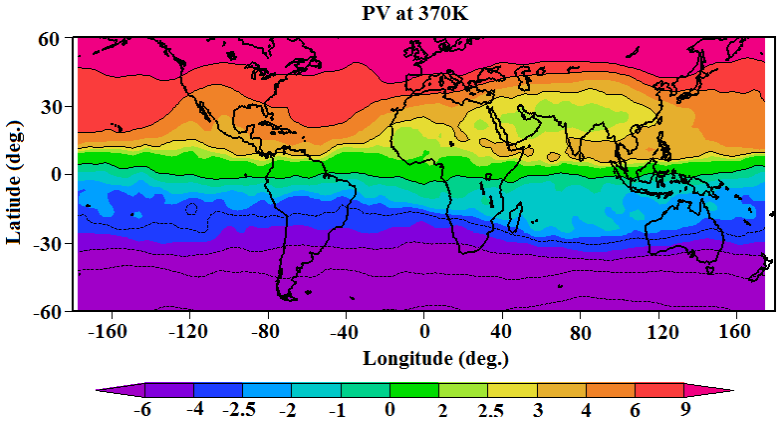

Figure 4. Panel **(a)** cross sections of seasonal mean ECHAM5-HAMMOZ NO_x (ppt) averaged for **(a)** 60–120° E, **(b)** 70–120° W, **(c)** 10–40° N, **(d)** 0–45° E and **(e)** 0–25° S. Panel **(b)** same as panel **(a)** but for HNO_3 (ppt).

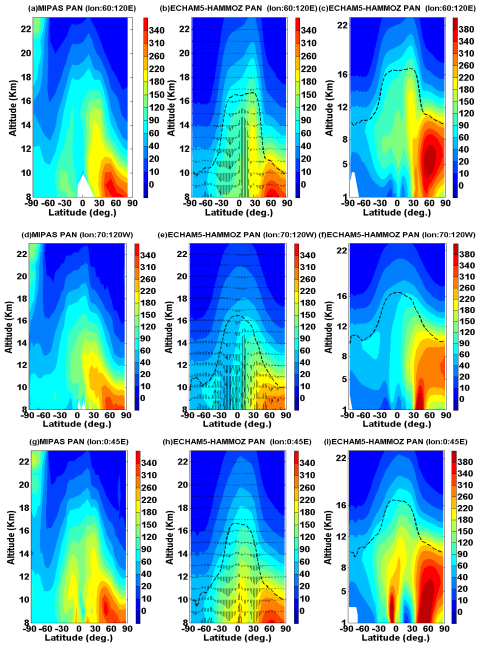

Figure 5. Latitude-altitude cross section of PAN (ppt) **(a)** MIPAS-E climatology (between 8–23 km), averaged for monsoon season and 60–120° E, **(b)** PAN from ECHAM5-HAMMOZ CTRL simulations, between 8–23 km, averaged for monsoon season and 60–120° E, **(c)** same as figure **(b)** but from the surface. **(d)** same as **(a)** but averaged over 70–120° W **(e)** same as **(b)** but averaged over 70–120° W **(f)** same as **(e)** but from the surface **(g)** same as **(a)** but averaged over 0–45° E **(h)** same as **(b)** but averaged for 0–45° E **(i)** same as figure **(h)** but from the surface. Wind vectors are indicated by black arrows in figures **(b)**, **(e)** and **(f)**. The vertical velocity field has been scaled by 300.

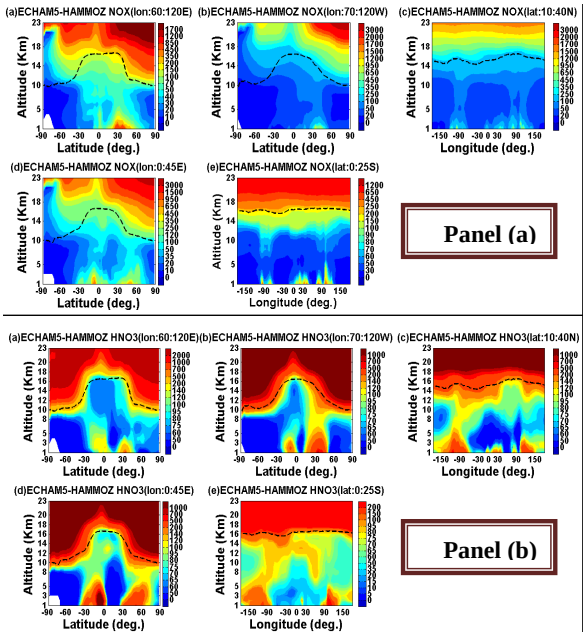

Figure 6. Panel **(a)** Latitude-altitude cross section of seasonal mean ECHAM5-HAMMOZ NO_x (ppt) averaged for **(a)** 60–120° E, **(b)** 70–120° W, **(c)** 10–40° N, **(d)** 0–45° E and **(e)** 0–25° S. Panel **(b)** same as panel **(a)** but for HNO_3 (ppt).

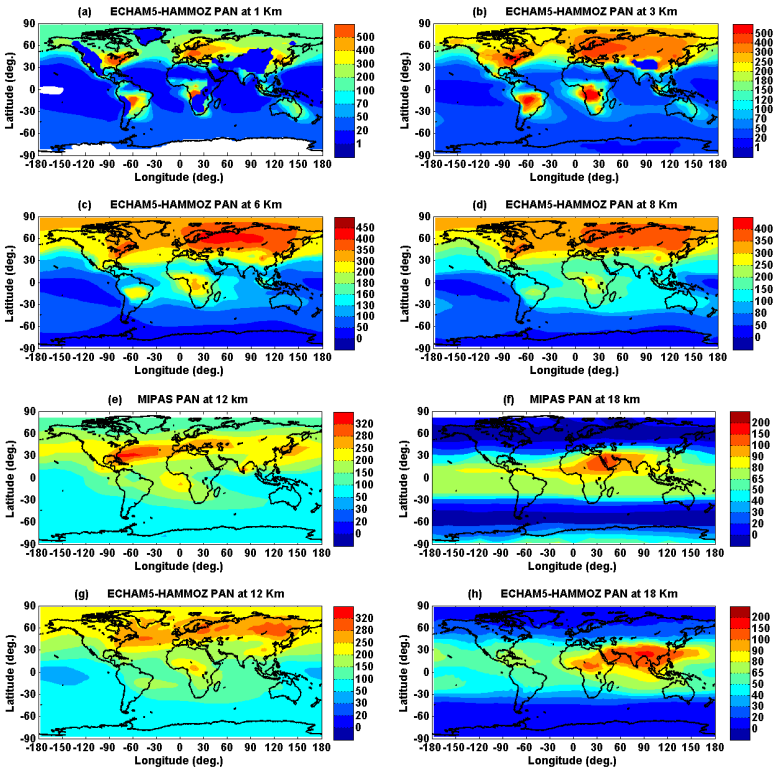

Figure 7. Latitude-longitude cross section of PAN (ppt) averaged for monsoon season **(a)** ECHAM5-HAAMOZ simulations at 1 km **(b)** 3 km **(c)** 6 km **(d)** 8 km. MIPAS-E climatology at **(e)** 12 km **(f)** 18 km. ECHAM5-HAMMOZ CTRL simulation at **(g)** 12 km **(h)** 18 km.

Discussion Paper | Discussion Paper | Discussion Paper | Discussion Paper |

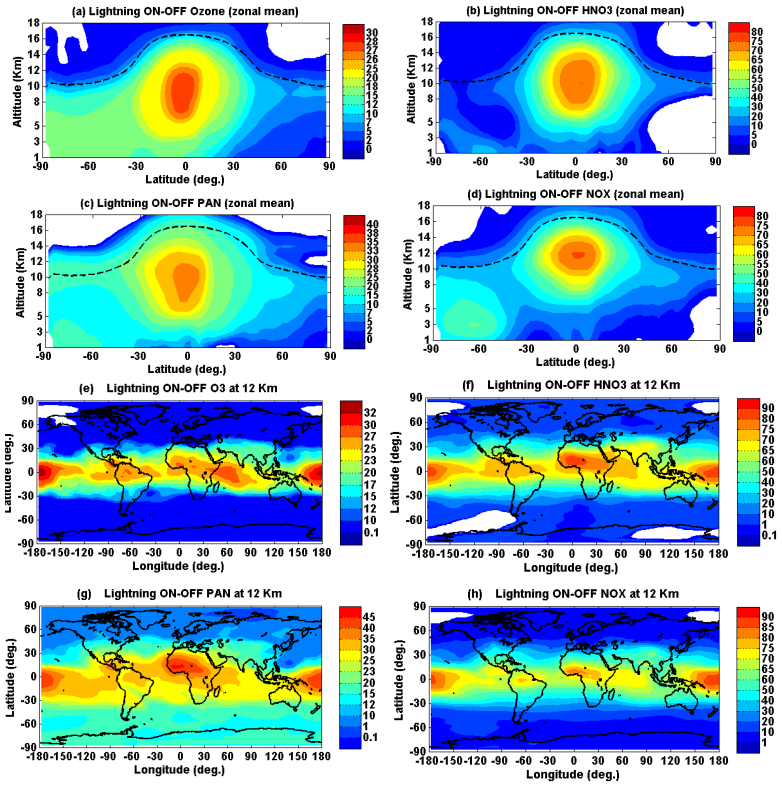

Figure 8. Zonally averaged seasonal mean changes (percentage) produced from lightning in **(a)** ozone **(b)** HNO_3 **(c)** PAN **(d)** NO_x, distribution of seasonal mean changes (percentage) produced from lightning in **(e)** ozone **(f)** HNO_3 **(g)** PAN **(h)** NO_x at 12 km.